# Fabrication and Characterization of Micromachined Active Probes With Polymer Membranes for Biomolecular Force Spectroscopy

Hamdi Torun, Krishna K. Sarangapani, and F. Levent Degertekin

***Abstract*—A micromachined polymer membrane-based active probe has been developed for biomolecular force spectroscopy. The probe has integrated but significantly decoupled electrostatic actuation and optical interferometric force sensing capabilities. Devices have been fabricated on silicon substrates using Parylene as the membrane material. The electrostatic actuator integrated into the probe could provide $>$ 1-$\mu$m displacement with a flat response of up to 30 kHz in fluid, a feature particularly useful in fast-pulling force spectroscopy experiments involving biomolecules. The probes were successfully employed to measure the unbinding forces between biotin and streptavidin, wherein the force noise level was $<$10 pN with a 1-kHz bandwidth for an 8-N/m membrane with a 25-kHz resonance frequency in fluid. This is in agreement with the thermal noise data generated by a finite-element model that predicts further improvements with simple design changes. [2010-0069]**

***Index Terms*—Atomic force microscopy, fabrication, microelectromechanical systems, molecular biophysics.**

## I. Introduction

ATOMIC force microscopy (AFM) has been widely used to measure the biological interaction forces in fluid [1]–[4]. In a conventional AFM system used for biomolecular force spectroscopy measurements, the force sensing element is a passive microcantilever functionalized with biomolecules of interest, whose kinetic and mechanical properties are being investigated. Unbinding/unfolding kinetics between the interacting biomolecules on the cantilever tip and an adjacent substrate are characterized by repeatedly moving the cantilever in and out of contact with the substrate using the piezo tube actuator of the AFM system, monitoring the bending of the cantilever (that corresponds to force) at all times. Commercially available AFM cantilevers can provide a force resolution of a few piconewtons (pN) with a 1-kHz bandwidth [5]. Force sensors with a lower inherent noise are needed to expand the capability of the AFM to probe different biomolecules and investigate interesting phenomena, such as the counterintuitive catch bonds in receptor–ligand interactions [6], [7]. The force resolution of an AFM system can be improved by using smaller cantilevers at the expense of microfabrication constraints and sophisticated detection systems that have hindered their use on a wide scale [8], [9].

Dynamic force spectroscopy measurements by varying the loading rate on the biomolecules allow researchers to investigate the energy landscapes governing the interactions [10]. The loading rate is heavily dependent on the pulling speed of the cantilever in a conventional AFM system. The hydrodynamic drag force on the moving cantilever increases as the pulling speed increases, which sets an upper bound on the maximum pulling speed before the hydrodynamic drag force becomes larger than the interaction force to be measured. This level is usually between 10 and 30 $\mu$m/s which is not adequate to completely map the energy landscapes [11]. Thus, novel actuators that enable measurements to have higher loading rates with minimal hydrodynamic drag forces on the force sensors are highly desirable.

Cantilevers are not the only force sensing structures suitable for AFM. Novel membrane and clamped-clamped beam structures with electrostatic actuation and integrated diffraction-based optical interferometric displacement detection capabilities have been recently introduced for AFM applications [12]. These probes, called the force-sensing integrated readout and active tip (FIRAT), have been designed to have a higher bandwidth compared to the slower commercially available cantilevers and have been used for several important AFM applications, such as fast imaging and capturing transient interaction forces between the probe tip and the sample, and for quantitative material characterization [13].

The use of a FIRAT probe structure as an actuator for biomolecular force spectroscopy has been demonstrated in liquid using sealed dielectric membranes made of silicon nitride/oxide layers [14]. These probes serve as fast electrostatic surface actuators coupled with cantilevers and have been designed for fabrication as arrays. A significant advantage of these actuators is that the hydrodynamic drag force induced on the cantilever is dramatically reduced, which enables the pulling of biomolecules that is an order of magnitude faster as compared with the regular cantilevers [15].

Although the optical displacement sensor integrated to those silicon nitride/oxide membrane actuators provided a noise floor

Manuscript received March 11, 2010; revised June 9, 2010; accepted July 15, 2010. This work was supported by the National Institutes of Health under Grant AI060799. Subject Editor C. Liu.

H. Torun is with the George W. Woodruff School of Mechanical Engineering, Georgia Institute of Technology, Atlanta, GA 30332-0405 USA.

K. K. Sarangapani is with the Department of Physiology and Biophysics, University of Washington, Seattle, WA 98195-7290 USA.

F. L. Degertekin is with the George W. Woodruff School of Mechanical Engineering and the School of Electrical and Computer Engineering, Georgia Institute of Technology, Atlanta, GA 30332 USA (e-mail: levent@gatech.edu).

Color versions of one or more of the figures in this paper are available online at http://ieeexplore.ieee.org.

Digital Object Identifier 10.1109/JMEMS.2010.2067439

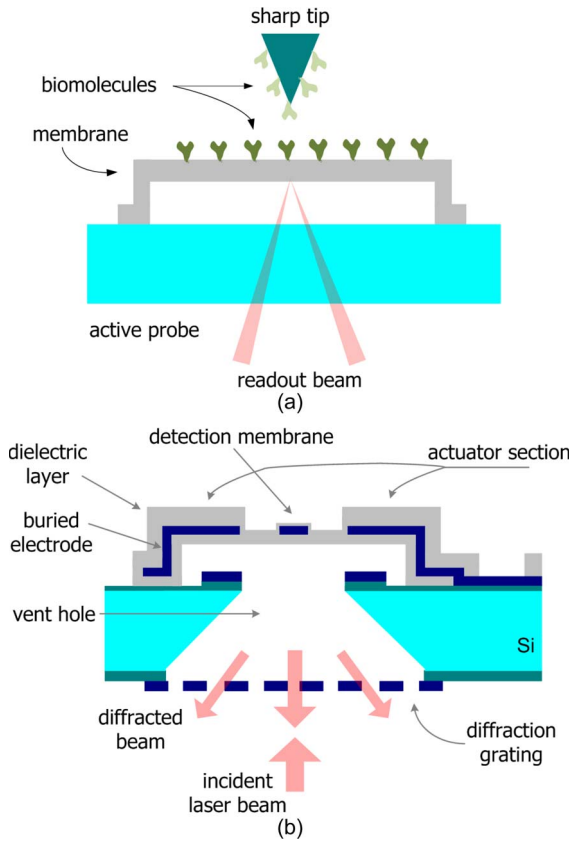


Fig. 1. (a) Generic schematic of a single-molecule experiment employing a functionalized active probe that is coupled with a functionalized sharp tip. (b) Schematic cross section of probe structure highlighting its different sections.

$< 10$ fm/$\sqrt{\text{Hz}}$ for the frequencies as low as 3 Hz, the force resolution was not adequate as a sensor. In this paper, we first describe the active probes with polymer membranes that combine sensing and actuation modalities for biomolecular force spectroscopy. The polymer membranes allow fabricating the compliant structures, enabling a better force resolution. We also present a nonuniform membrane design that significantly decouples the sensor from the actuator. The independently optimized sensor improves the performance of the probe when it is used for force sensing. In contrast to the earlier designs, the probe membrane sits on a silicon substrate with wafer holes that serve as venting holes for the membrane to overcome the squeezed film damping effects. We then describe the silicon-based fabrication process of these probes using the Parylene film and standard IC materials. We also discuss the noise performance of the probes through modeling and experimental characterization. Finally, we demonstrate the utility of these probes in biomolecular force spectroscopy experiments.

## II. Structure and Operation of Membrane-Based Active Probes

The generic schematic of a single molecule experiment using the membrane probe is shown in Fig. 1(a). In this setup, a sharp tip functionalized with the desired molecules localizes the interaction to the center of the membrane probe. When the probe is used as both an actuator and a force sensor, the tip should be stiff so as not to interfere with the force measurement. Alternatively, an AFM cantilever can be used as the force sensor while the membrane probe is used as an actuator [14]. The sharp tip can be positioned in the $X$–$Y$ and $Z$ using a conventional piezo actuator. The distance between the interacting biomolecules is controlled using the piezo actuator of the tip and the electrostatic actuator of the membrane. The unbinding forces are monitored using the optical displacement sensor integrated to the probe.

The cross section of an active probe developed for in-fluid operation is schematically shown in Fig. 1(b). The circular probe membrane sits on a silicon substrate. A nonuniform membrane structure design optimizes the performance of the actuator and the sensor simultaneously. The thicker side of the membrane is the actuator section. It forms the parallel-plate-type electrostatic actuator integrated to the probe. Moving the electrodes to the sides extends the actuation range of a uniform parallel-plate-type electrostatic actuator for which the range is typically one-third of the gap height [16]. The top electrode of the actuator is sealed with a thicker dielectric layer. This layer provides a better electrical insulation when the buried electrode is electrically excited. The thicker actuator section also makes a relatively stiff actuator. This increases the resonant frequency of the actuator and enables fast-pulling experiments. Moving the electrodes to the sides and increasing the dielectric layer thickness come at the expense of higher, but reasonable, voltage levels needed to move the membrane.

The center part of the probe forms the detection membrane for force sensing. This part can be thinner (hence more compliant), leading to a nonuniform membrane structure. It is mainly made of a thin dielectric layer with a circular metal layer. This metal layer serves as the second reflector forming the diffraction grating interferometer that measures the displacement of the membrane. When a laser beam illuminates the membrane from the back, the light reflects off the membrane and interferes with the light reflecting off the diffraction grating attached to the bottom of the substrate. The reflected light goes into diffraction orders due to the grating. The intensity of the light at the diffraction orders is a sinusoidal function of the gap between the membrane and the diffraction grating. Further details of the detection method can be found elsewhere [17]. It should be noted that the diffraction grating is placed at the back of the silicon substrate in this design and is not an integrated part of the probe. Replacing the grating with a semitransparent mirror forms a simple Michelson interferometer. It is also possible to combine the probe with a tunable grating device [18]. A tunable grating guarantees that the interferometer operates at its maximum sensitive point independent of the position of the membrane.

The vent hole under the membrane not only provides optical access for the interferometer but also allows the fabrication of a free-standing membrane. The membranes are released from the back using vent holes as described in the next section. This approach eliminates the need for an etch channel on the front side of the probe, which is exposed to the fluid. Sealing such etch channels may be difficult without affecting the characteristics of the probes. The vent hole also equalizes the pressure between both sides of the probe, which, in turn, makes the probe

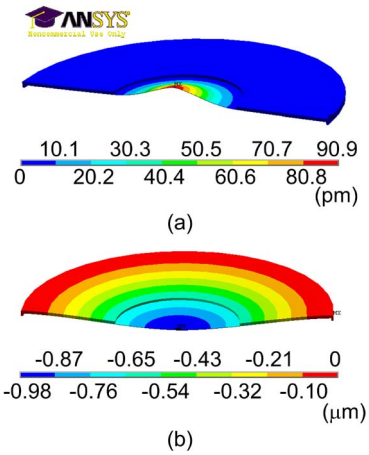


Fig. 2. FEM simulation of displacement profile of (a) the unbiased membrane when 100-pN point force is applied at the center and of (b) the membrane with applied voltage to the side electrodes to displace the center by 1 $\mu$m. One-half of the membrane is shown.

immune to ambient pressure gradients that might displace the membrane during its operation. More importantly, the detection membrane has no rigid structure underneath it owing to the vent hole. Thus, the force sensor is minimally affected by the squeezed film damping due to the gas film trapped between the moving membrane and the rigid substrate. The squeeze film damping adversely alters the dynamics of the microstructures and increases the level of thermal noise [19].

In a typical biological experiment as described in Fig. 1, the detection membrane is used to sense the point forces acting at its center. One needs a compliant detection membrane to increase the force sensitivity. This membrane also should be small to reduce the thermal noise due to viscous damping. For decoupled operation, this point force should not affect the thicker actuator section. Similarly, when the actuator is activated, the properties of the detection membrane, such as the force sensitivity, should not change. A finite element method (FEM) has been used to design and simulate the decoupled membrane structure. An axisymmetric model using the commercial software ANSYS is used to analyze both cases. The probe in this model is 300 $\mu$m in diameter with a 120-$\mu$m-diameter detection membrane. The detection membrane is 0.5 $\mu$m thick, and the actuation section is 3 $\mu$m thick. The computational domain is composed of a 2-D structural element, the Plane82. A point force of 100 pN was applied at the probe center after clamping the edges. The center of the detection membrane displaces 91 pm while the deflection of the actuation section is negligible [see Fig. 2(a)].

Next, we analyzed the effect of the actuator on the detection membrane. First, we calculated a stiffness of 1.1 N/m for the unbiased membrane through FEM simulations. Then, we biased the actuator so that the center of the membrane is displaced by 1 $\mu$m as shown in Fig. 2(b). We used an electrostatic element, the Plane121, for this electrostatic-structural coupled-field analysis. The initial gap of the membrane is 2.5 $\mu$m. For the case of the actuated membrane, the stiffness of the detection membrane changes—it is actually reduced—only by 2.2%. Hence, the use of rigid side electrodes for the actuation does not significantly alter the behavior of the sensor membrane. On the other hand, an electrostatic actuator with uniform electrodes would alter the stiffness significantly due to the spring softening effect [20]. To summarize, the nonuniform membrane structure allows us to make smaller and compliant detection membranes, together with sealed rigid actuators. The FEM simulations show that the operation of the sensor and actuator does not impact each other, indicating a decoupled sensor/actuator combination.

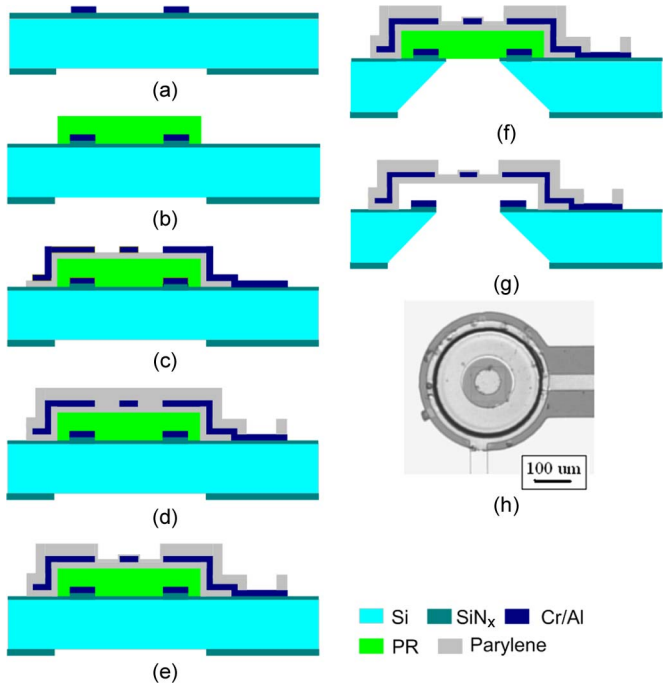


Fig. 3. Process flow for the microfabrication of membranes and top view of a fabricated membrane. (a) Nitride deposition and patterning on both sides, bottom electrode definition. (b) Thining down the front side nitride, PR sacrificial layer definition. (c) Bottom Parylene definition, top electrode definition. (d) Top Parylene definition. (e) (Optional) Thinning down the detection membrane. (f) KOH-etching of Si, RIE-etching of front side nitride from backside. (g) Releasing in acetone. (h) Photograph of a 300-$\mu$m-diameter membrane.

## III. Fabrication of Probe Membranes

The microfabrication of the probe membranes is a Si-based seven-mask process as schematically illustrated in Fig. 3. We fabricated probe membranes on a 300-$\mu$m-thick Si wafer. The fabrication process started with the deposition of 3-$\mu$m-thick plasma-enhanced chemical deposition nitride films on both sides of the wafer. We used the back-side nitride film as a mask for etching the silicon substrate using potassium hydroxide (KOH) in a subsequent step. The front-side nitride film electrically isolates the electrodes from each other and the substrate. On top of this nitride layer, we patterned 100-nm-thick gold electrodes (with 10-nm-thick chromium as an adhesion layer). For this step, we used a filament evaporator and a standard liftoff process with the first mask as shown in Fig. 3(a). These electrodes serve as the bottom electrodes of the electrostatic actuators integrated to the membrane probes. After the definition of the bottom electrodes, we patterned the back-side nitride layer in a reactive ion etch (RIE) chamber to open the KOH etching windows with the second mask. The back-side alignment was required for this lithography step to align the

windows to the electrodes on the front side of the wafer. Then, we thinned the front-side nitride layer down to a thickness of 1 $\mu$m. We spun and patterned a 2.5-$\mu$m-thick sacrificial photoresist (PR) (SC1827, Shipley) as shown in Fig. 3(b). We started to build the membrane with a 0.5-$\mu$m-thick chemical-vapor-deposited Parylene layer deposition. This layer is an insulation layer between the electrodes to avoid electrical shorting in case of membrane collapse. This Parylene layer is also the structural layer for the detection membrane. We patterned the Parylene layer using the oxygen plasma in a RIE chamber. We used a titanium hard mask for the RIE etching since the etch rates of the Parylene and PR are on the same order with the oxygen plasma. The titanium hard mask layer was sputtered to a thickness of 70 nm. After the oxygen plasma, this layer was removed using diluted hydrofluoric acid (HF). The etching solution was prepared by adding 15 drops (using a disposable Pasteur pipette and with a drop size of 20–50 $\mu$L) of 45% HF into 300 mL of deionized water. We did not observe the HF attacking the other layers since it was very diluted and etched the titanium layer fast. Then, we sputtered a 150-nm-thick aluminum layer that serves as the top electrodes. In order to promote adhesion between the aluminum and Parylene layers, we sputtered 10-nm-thick chromium layers on the top and bottom sides of the aluminum layer. We wet etched the metal layers as shown in Fig. 3(c). For the chromium etching, we used the chromium etchant type 1020 (Transene Company Inc., Danvers, MA) at room temperature. For the aluminum etching, we used the aluminum etchant type A (Transene Company Inc., Danvers, MA) at 50 °C. Finally, we deposited a 1-$\mu$m-thick Parylene layer over the top electrodes. This layer protects the electrodes in the fluid. This Parylene layer is also where the biomolecules are anchored in biological experiments. We patterned the top Parylene layer similarly using the oxygen plasma with a titanium hard mask [see Fig. 3(d)]. For the uniform membrane, the fabrication of the front side of the wafer ends after this step. To define the nonuniform membranes with a thinner center part, we thinned down the top Parylene layer using oxygen plasma as shown in Fig. 3(e). Then, we opened the back-side venting holes using KOH as shown in Fig. 3(f). The front side of the wafer was protected using a commercial wafer holder (AMMT GmbH, Frankenthal, Germany). The venting holes also serve as the etch holes to release the membranes. The KOH bath was held below 70 °C to prevent cracking on the Parylene layers due to thermal stress. In addition, we also carried out all the hard-baking and soft-baking steps below 90 °C after the deposition of the first Parylene layer. Otherwise, we observed cracking on the membrane layers. The anisotropic etching of the silicon substrate with KOH stopped at the front side nitride layer, which we removed using the RIE from the back side of the wafer. Finally, we diced the wafers into chips and released the membranes in acetone. We dried the samples using a supercritical dryer to prevent stiction after the PR layer was removed.

The surface of the membrane is Parylene, which is hydrophobic in nature. During the membrane functionalization in biomolecular experiments, it is absolutely mandatory that the membrane surface be able to anchor the biomolecules without compromising on the molecular functionality. The surface properties of Parylene can be altered by oxygen plasma treatment in a RIE chamber [21]. Hence, the surface chemistry of a hydrophobic Parylene surface can be accordingly altered for experiments involving protein adsorption or bilayer-reconstituted membrane proteins. The treated Parylene surface can retain its properties for a few days [22], [23]. This is an advantage over the other polymers, such as the polydimethylsiloxane for which plasma treatment effects last only for a few hours. The probe membranes are reusable. After a biological experiment, the membrane surface can be cleaned using organic solvents, and if needed, the polymer surface can be plasma treated again.

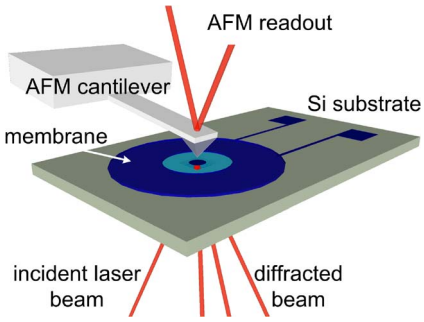


Fig. 4. Schematic of membrane probe coupled with AFM cantilever in the experimental setup.

## IV. Experimental Characterization and Modeling

We characterized the fabricated probes in air and in fluid, ensuring that they performed well during the force spectroscopy experiments. Here, we present the experimental characterization and biomolecular force spectroscopy data using both the uniform and nonuniform membranes. Based on the experimental data that we have gathered, we also present projections regarding the performance of the probes with this design. The experimental characterization setup used for the characterization of the probes is shown in Fig. 4 where an AFM cantilever is coupled to a membrane probe. The cantilever is controlled with a commercial AFM system (Nanoscope 3100, Veeco Metrology–Digital Instruments, Santa Barbara, CA).

Biomolecular experiments investigating protein–protein, antigen–antibody, or ligand–receptor interactions typically require a pulling range of $\sim$1 $\mu$m before the bond rupture or the domain unfolding [24]. The membrane probes are capable of delivering the required displacement range. The range of the electrostatic actuator depends on the gap between the membrane and the substrate [labeled as $d_0$ in Fig. 5(a)]. We measured the range provided by a 200-$\mu$m-diameter 2.5-$\mu$m-thick uniform membrane by engaging an AFM cantilever at the center of the membrane using the experimental setup shown in Fig. 2. The spring constant of the membrane was 150 N/m, and that of the cantilever was 0.01 N/m. Since the membrane was much stiffer than the cantilever, the loading of the cantilever on the membrane due to the engaged cantilever was negligible. Initially, the cantilever was indented around 3 $\mu$m on the membrane. Then, the bias voltage between the electrodes of the membrane actuator was gradually increased. Since the membrane and the cantilever were fully in contact, the soft cantilever followed the membrane displacement. We continually

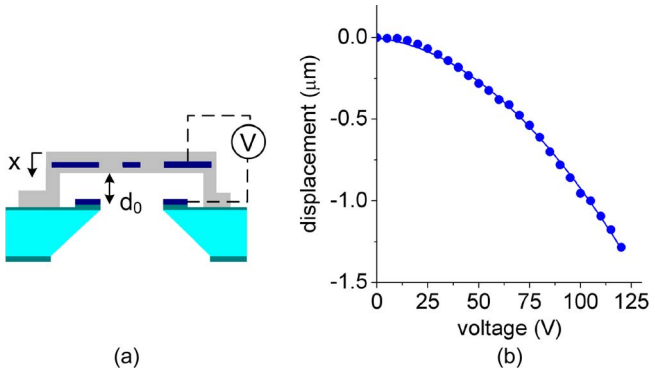


Fig. 5. (a) Schematic of integrated electrostatic actuator with side electrodes. (b) Displacement of a 200-$\mu$m-diameter membrane with applied bias voltage.

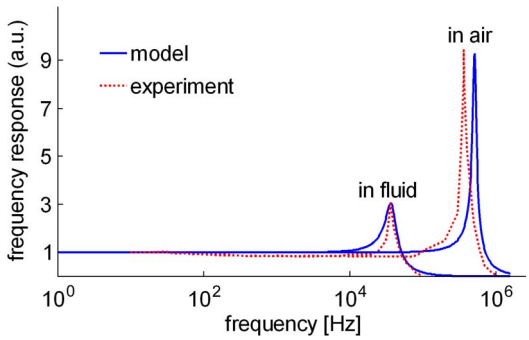


Fig. 6. Frequency response of a 200-$\mu$m-diameter membrane in air and fluid.

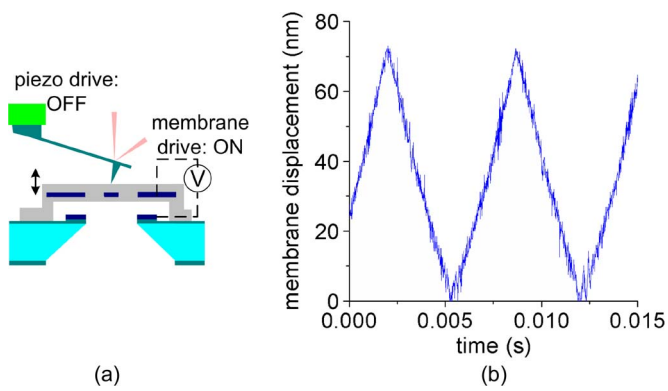


Fig. 7. (a) Actuation of an AFM cantilever by using electrostatic actuator of membrane probe. (b) Cantilever readout signal in fluid when the membrane was actuated by a ramp signal.

monitored the deflection of the cantilever using the optical lever readout of the AFM system. Fig. 5(b) shows that the membrane was displaced $> 1.25$ $\mu$m [labeled as $x$ in Fig. 5(a)] before it collapsed to the substrate. The initial gap height was 2.5 $\mu$m. A simple parallel-plate electrostatic actuator with uniform electrodes at the same gap height would provide a range of 0.83 $\mu$m before collapsing. Thus, we observed a 50% improvement regarding the displacement range with these probe actuators using the side electrodes. The whole range required less than 125-V bias. This level is comparable to the requirements of the piezo tube actuators commonly used in commercial AFM systems.

The outlined method of the actuator characterization is ideal for our proposed application. We can measure the displacement of the membrane exactly at a single point where the biomolecular interactions are most likely to occur. This method is employed to calibrate the membrane actuators before any biological experiment. Calibrating the actuators minimizes any uncertainties due to the unwanted effects, such as the parasitic charge accumulation that alters the characteristics of electrostatic actuators [25].

The actuation speed provided by piezo tube actuators is not enough for fast-pulling experiments. Novel actuation methods, such as integrated micromachined piezoelectric actuators or photothermal cantilever actuators, have been developed to overcome the shortcomings of the piezo tube actuators [26], [27]. Using these methods, the actuation bandwidth of the cantilevers in liquid has been extended to a few tens of kilohertz.

The electrostatic actuator integrated to the membrane probe is a fast actuator. The bandwidth of the electrostatic actuator can provide high pulling rates since the speed is determined by the membrane dynamics. Fig. 6 shows the experimentally obtained frequency response of a 200-$\mu$m-diameter actuator. We drove this membrane with an ac voltage imposed on top of a dc bias voltage and measured its displacement using the diffraction grating interferometer of the probe. We measured a resonant frequency of 365 kHz in air, which was predicted well using a single-harmonic oscillator lumped model. The resonant frequency of the same membrane dropped to 36 kHz in fluid. The drop in the resonant frequency can be explained well by incorporating the loading effect of the fluid on the vibrating membrane on a lumped element model. [28]. We also introduced additional damping to the model to match the quality factor measured experimentally. The flat response until the resonant frequency ensures the effective use of the actuator for fast-pulling experiments.

We demonstrated the use of membrane probes to actuate the cantilevers in fluid by engaging a cantilever at the center of the membrane and keeping it fully in contact with the membrane. We drove the membrane at a speed of 21 $\mu$m/s and read the displacement of the cantilever as shown in Fig. 7. A membrane driven at 5 kHz with a triangular 1-$\mu$m peak-to-peak waveform will provide a rate of $10^4$ $\mu$m/s. This is more than an order of magnitude faster than that possible with conventional AFM. In addition to a faster actuation, the cantilever feels very low hydrodynamic drag forces when moved by a membrane actuator as compared to the cantilever itself being actuated with a piezo tube actuator or when a sample stage is actuated against the cantilever [15]. Thus, the whole bandwidth of the electrostatic actuator can be exploited to map the energy landscapes of molecular systems. The details of this drive scheme and supporting experimental data have been reported [15].

When used as a force sensor, the membranes should be designed carefully to minimize noise. We conducted experimental and modeling studies to understand the noise characteristics of the polymer membranes when immersed in fluids. The fundamental noise sources in the system can be identified as the thermal noise of the membranes and the shot noise in the photodetectors.

To understand the thermal noise contributions, we modeled the noise behavior of the membranes using an FEM model based on the commercial software COMSOL. This model can

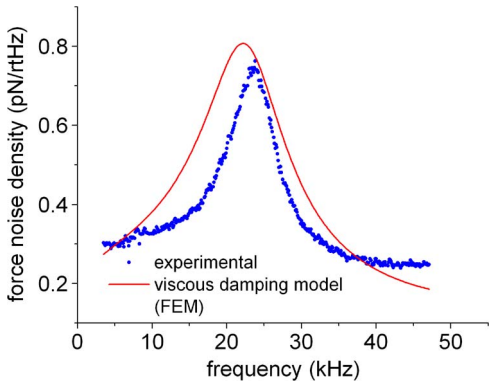


Fig. 8. Force noise spectrum of a 500-$\mu$m-diameter force probe with 300-$\mu$m-diameter detection membrane in fluid.

be used to solve the Navier–Stokes equations to extract the frequency-dependent viscous damping on a membrane in fluid due to the hydrodynamic drag force. Calculating the viscous damping allows us to generate the thermal noise spectra without the need for a fitting parameter prior to any experimental characterization. To calculate the shot noise level for a particular membrane sensor, we measured the photocurrent in the photodiodes. The outer diameter of the membrane used in the experiments was 500 $\mu$m. The detection membrane was 300 $\mu$m in diameter. Its spring constant was measured to be 8 N/m. Based on these values, we calculated a shot noise level of 0.13 pN/$\sqrt{}$Hz below 1 kHz.

We measured the force noise spectra of this membrane in fluid and compared it with our noise model results in Fig. 8. For the particular membrane, we predicted a thermal noise below 1 kHz to be 0.22 pN/$\sqrt{}$Hz, which is in good agreement with the measurements and validates the FEM-based model.

The total noise floor of the presented membrane in fluid is 8.1 pN with a 1-kHz detection bandwidth. The force resolution of the current probes is comparable to that of the commercially available cantilevers. For example, the thermal noise floor of a 200-$\mu$m-long rectangular cantilever (from Veeco Instruments Inc.) with a nominal spring constant of 0.02 N/m is 8.4 pN with a 2-kHz bandwidth in fluid [29].

For a comparison of the force curves, we captured the displacements of a membrane probe and an AFM cantilever simultaneously. We coupled this 500-$\mu$m-diameter force probe with a rectangular silicon cantilever (force modulation etched silicon probe (FESP), Veeco Instruments Inc.) in fluid. The nominal spring constant of this cantilever is 2.8 N/m which is comparable to that of the membrane probe. Moreover, the resonant frequency of a FESP tip was previously reported to be 30 kHz in fluid, which is also similar to that of our probe [30].

We actuated the FESP cantilever in and out of contact with the probe membrane and captured the force curves simultaneously. Fig. 9 shows the captured force curves when we set the peak force on the cantilever such that the signal-to-noise ratio (SNR) was unity. The results show that a membrane probe can have a lower noise as compared to a typical AFM cantilever with similar mass and spring constant.

The force resolution of the membrane probes can be further improved using thinner detection membranes. The lower spring constant of the thinner membrane will increase the force sensitivity which reduces the shot noise component of the force noise. The lateral size of the membrane can be reduced to achieve the same stiffness with a thinner membrane. Minimizing the moving area will reduce the viscous damping of the structure, and this will help reduce the thermal noise component of the force noise. The projection based on the experimental results obtained with the current membranes and the FEM-based model used to predict the viscous damping is that it is possible to measure interaction forces of 0.3–1 pN with a 1-kHz bandwidth in fluid using the membranes with spring constants of 1–5 N/m. Fabricating thinner membranes is challenging. Thinner layers are prone to cracking and delaminating due to residual and thermal stresses. Controlling the thickness uniformity is also crucial with thinner layers. Therefore, alternative materials in addition to Parylene should also be evaluated for fabricating thinner membranes.

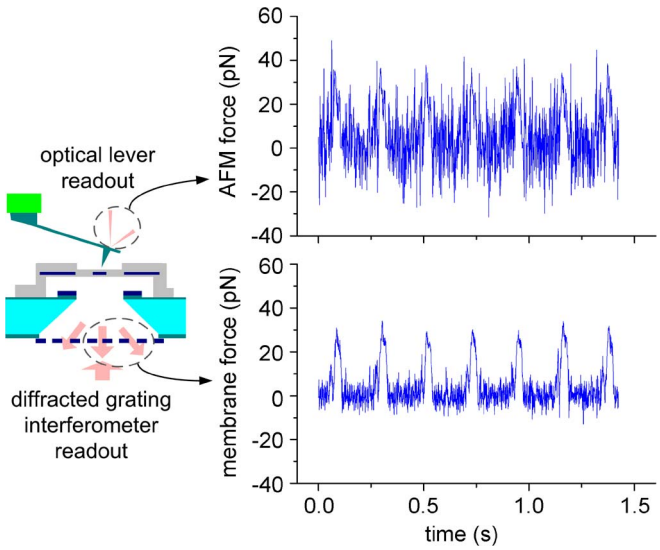


Fig. 9. Comparison of force curves obtained by the AFM cantilever and the membrane probe when a 2.8-N/m cantilever with quality factor of 3.8 was actuated against an 8-N/m membrane in fluid. The peak force on the cantilever was set such that SNR = 1.

## V. Biological Experiments With the Membrane Probes

We measured the unbinding forces between biotin and streptavidin to demonstrate the use of these membrane probes in biomolecular force spectroscopy experiments. In these experiments, we selected a cantilever with a spring constant of 14 N/m that was prefunctionalized with biotin (CT. BIO, Novascan Technologies, Inc., Ames, IA). After removing the cantilever from the sealed pack, it was incubated with $\sim$20 $\mu$l of streptavidin (10 $\mu$g/ml) that has an extremely strong affinity for biotin, and the 500-$\mu$m-diameter probe membrane was functionalized with biotinylated bovine serum albumin (BSA). The membrane was then covered with Dulbecco's phosphate-buffered saline solution (Sigma-Aldrich Inc., St. Louis, MO). Streptavidin is a symmetric tetrameric protein and has four binding sites for biotin [31]. Due to its structural symmetry, we believe that two of those sites would be used to strap them onto the biotin on the AFM cantilever, leaving the other two sites free for binding

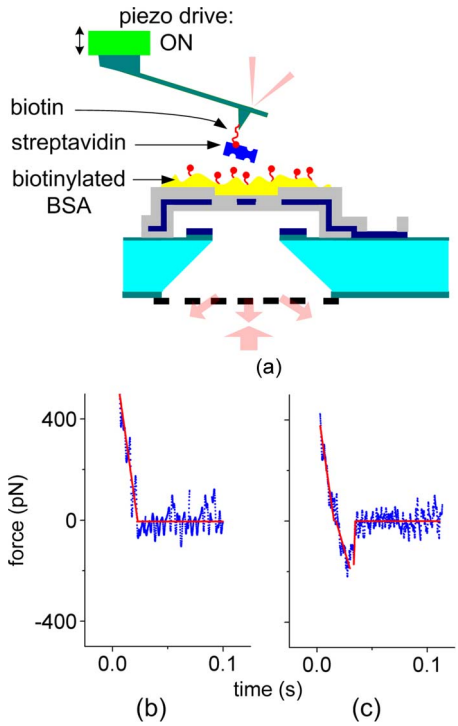


Fig. 10. (a) Functionalized AFM cantilever tested against a membrane probe. Prefunctionalized AFM cantilever was incubated with streptavidin while the membrane probe was functionalized with biotinylated BSA. (b) Sample force curve showing a null adhesion event. Force on the membrane stays at zero immediately after the membrane gets out of contact with the AFM cantilever. (c) Sample force curve showing a 200-pN unbinding event, as signified by the negative "dip" of the force trace, immediately when the membrane and the cantilever are out of contact. In this case, the membrane and cantilever are still linked by a biomolecular bond.

with the BSA on the membranes. By exploiting these structural properties, streptavidin can be used as a nanoscale building block [32]. Incubating the membranes with the BSA helped block the rest of the surface, which helped minimize nonspecific interactions.

We performed experiments by repeatedly moving the AFM cantilever with the piezo actuator of the commercial AFM system at 2 Hz while the probe membrane was kept stationary. Fig. 10 shows the typical force curves that we captured using the membrane sensor, wherein a zero mean force indicates that the cantilever and the membrane are out of contact. We detected a positive force value when the cantilever pushes into the membrane. Negative force values correspond to the interacting forces between the biomolecules that are manifest on the membrane as a deflection. Fig. 10(b) shows a force curve with no unbinding event as the force stayed at zero position immediately after the membrane got out of contact with the cantilever. Fig. 10(c) shows a sample force curve with a specific unbinding event. The strength of the interaction was $\sim$200 pN. The adhesion frequency (i.e., the fraction of binding events in 100 repeated test cycles) was between 30%–40%. At such a binding frequency, the bulk of the interactions would involve single molecular pairs, according to small number statistics. The findings that we obtained here are in good agreement with the data presented previously using similar Parylene membranes [33].

## VI. Conclusion

Active force probes with polymer membranes have been fabricated on silicon wafers. These probes have the desired dynamics and noise characteristics for fast high-resolution biomolecular force measurements. The integrated electrostatic actuator of the probe provides $> 1$ $\mu$m vertical range with side electrodes, which is ideal for biomolecular force spectroscopy experiments. The actuator's speed is determined solely by the membrane dynamics that is over an order of magnitude faster than that of the commercial AFM systems while generating virtually no hydrodynamic drag [15]. The speed and range of this actuator make it a good candidate for applications requiring fast feedback controlled systems [34]. The fabrication process of these probes allows for the simultaneous optimization of the sensor and actuator characteristics. For example, nonuniform membrane probes with a thin center and thick outer sections provide compliant low noise sensing and fast rigid actuation capabilities, respectively. The initial results obtained with these devices involving the biotin and streptavidin strongly suggest that their force resolution is comparable to that of the commercially available cantilevers. With relatively simple structural changes, we believe that the force resolution of the sensor can be significantly improved.

## Acknowledgment

The authors would like to thank O. Finkler for his help with the data acquisition setup.

## References

[1] U. Dammer, M. Hegner, D. Anselmetti, P. Wagner, M. Dreier, W. Huber, and H. J. Guntherodt, "Specific antigen/antibody interactions measured by force microscopy," *Biophys. J.*, vol. 70, no. 5, pp. 2437–2441, May 1996.

[2] E.-L. Florin, V. T. Moy, and H. E. Gaub, "Adhesion forces between individual ligand-receptor pairs," *Science*, vol. 264, no. 5157, pp. 415–417, Apr. 1994.

[3] P. Hinterdorfer and Y. F. Dufrene, "Detection and localization of single molecular recognition events using atomic force microscopy," *Nat. Methods*, vol. 3, no. 5, pp. 347–355, May 2006.

[4] B. T. Marshall, K. K. Sarangapani, J. Lou, R. P. McEver, and C. Zhu, "Force history dependence of receptor-ligand dissociation," *Biophys. Soc.*, vol. 88, no. 2, pp. 1458–1466, Feb. 2005.

[5] K. C. Neuman and A. Nagy, "Single-molecule force spectroscopy: Optical tweezers, magnetic tweezers and atomic force microscopy," *Nat. Methods*, vol. 5, no. 6, pp. 491–505, Jun. 2008.

[6] B. T. Marshall, M. Long, J. W. Piper, T. Yago, R. P. McEver, and C. Zhu, "Direct observation of catch bonds involving cell-adhesion molecules," *Nature*, vol. 423, no. 6936, pp. 190–193, May 8, 2003.

[7] K. K. Sarangapani, T. Yago, A. G. Klopocki, M. B. Lawrence, C. B. Fieger, S. D. Rosen, R. P. McEver, and C. Zhu, "Low force decelerates L-selectin dissociation from P-selectin glycoprotein ligand-1 and endoglycan," *J. Biol. Chem.*, vol. 279, no. 3, pp. 2291–2298, Jan. 16, 2004.

[8] T. E. Schaffer and P. K. Hansma, "Characterization and optimization of the detection sensitivity of an atomic force microscope for small cantilevers," *J. Appl. Phys.*, vol. 84, no. 9, pp. 4661–4666, Nov. 1998.

[9] M. B. Viani, T. E. Schaffer, A. Chand, M. Rief, H. E. Gaub, and P. K. Hansma, "Small cantilevers for force spectroscopy of single molecules," *J. Appl. Phys.*, vol. 86, no. 4, pp. 2258–2262, Aug. 1999.

[10] R. Merkel, P. Nassoy, A. Leung, K. Ritchie, and E. Evans, "Energy landscapes of receptor-ligand bonds explored with dynamic force spectroscopy," *Nature*, vol. 397, no. 6714, pp. 50–53, Jan. 1999.

[11] H. Janovjak, J. Struckmeier, and D. J. Müller, *Hydrodynamic Effects in Fast AFM Single-Molecule Force Measurements*. New York: Springer-Verlag, 2005, pp. 91–96.

[12] A. G. Onaran, M. Balantekin, W. Lee, W. L. Hughes, B. A. Buchine, R. O. Guldiken, Z. Parlak, C. F. Quate, and F. L. Degertekin, "A new atomic force microscope probe with force sensing integrated readout and active tip," *Rev. Sci. Instrum.*, vol. 77, no. 2, p. 023501, Feb. 2006.

[13] M. Balantekin, A. G. Onaran, and F. L. Degertekin, "Quantitative mechanical characterization of materials at the nanoscale through direct measurement of time-resolved tip-sample interaction forces," *Nanotechnology*, vol. 19, no. 8, p. 85704, Feb. 2008.

[14] H. Torun, J. Sutanto, K. K. Sarangapani, P. Joseph, F. L. Degertekin, and C. Zhu, "A micromachined membrane-based active probe for biomolecular mechanics measurement," *Nanotechnology*, vol. 18, no. 16, p. 165303, Apr. 25, 2007.

[15] K. Sarangapani, H. Torun, O. Finkler, C. Zhu, and L. Degertekin, "Membrane-based actuation for high-speed single molecule force spectroscopy studies using AFM," *Eur. Biophys. J.*, vol. 39, no. 8, pp. 1219–1227, Jul. 2010.

[16] E. S. Hung and S. D. Senturia, "Extending the travel range of analog-tuned electrostatic actuators," *J. Microelectromech. Syst.*, vol. 8, no. 4, pp. 497–505, Dec. 1999.

[17] N. A. Hall, W. Lee, and L. Degertekin, "Capacitive micromachined ultrasonic trransducers with diffraction-based integrated optical displacement detection," *IEEE Trans. Ultrason., Ferroelectr., Freq. Control*, vol. 50, no. 11, pp. 1570–1580, Nov. 2003.

[18] O. G. Karhade, F. L. Degertekin, and T. R. Kurfess, "SOI-based micro scanning grating interferometers: device characterization, control and demonstration of parallel operation," *J. Micromech. Microeng.*, vol. 18, no. 4, p. 045007, Apr. 2008.

[19] T. Veijola, H. Kuisma, and J. Lahdenperä, "The influence of gas-surface interaction on gas-film damping in a silicon accelerometer," *Sens. Actuators A, Phys.*, vol. 66, no. 1–3, pp. 83–92, Apr. 1998.

[20] H. Torun, K. K. Sarangapani, and F. L. Degertekin, "Spring constant tuning of active atomic force microscope probes using electrostatic spring softening effect," *Appl. Phys. Lett.*, vol. 91, no. 25, pp. 253 113-1–253 113-3, Dec. 2007.

[21] S. Alvarez-Blanco, S. Manolache, and F. Denes, "A novel plasma-enhanced way for surface-functionalization of polymeric substrates," *Polymer Bull.*, vol. 47, no. 3/4, pp. 329–336, Dec. 2001.

[22] T. Y. Chang, V. G. Yadav, S. De Leo, A. Mohedas, B. Rajalingam, C.-L. Chen, S. Selvarasah, M. R. Dokmeci, and A. Khademhosseini, "Cell and protein compatibility of Parylene-C surfaces," *Langmuir*, vol. 23, no. 23, pp. 11 718–11 725, Nov. 2007.

[23] S. Selvarasah, S. H. Chao, C. L. Chen, S. Sridhar, A. Busnaina, A. Khademhosseini, and M. R. Dokmeci, "A reusable high aspect ratio parylene-C shadow mask technology for diverse micropatterning applications," *Sens. Actuators A, Phys.*, vol. 145/146, pp. 306–315, Jul./Aug. 2008.

[24] K. J. Van Vliet, G. Bao, and S. Suresh, "The biomechanics toolbox: Experimental approaches for living cells and biomolecules," *Acta Mater.*, vol. 51, no. 19, pp. 5881–5905, Nov. 2003.

[25] J. Wibbeler, G. Pfeifer, and M. Hietschold, "Parasitic charging of dielectric surfaces in capacitive microelectromechanical systems (MEMS)," *Sens. Actuators A, Phys.*, vol. 71, no. 1/2, pp. 74–80, Nov. 1998.

[26] T. Sulchek, R. Hsieh, J. D. Adams, S. C. Minne, C. F. Quate, and D. M. Adderton, "High-speed atomic force microscopy in liquid," *Rev. Sci. Instrum.*, vol. 71, no. 5, pp. 2097–2099, May 2000.

[27] H. Yamashita, N. Kodera, A. Miyagi, T. Uchihashi, D. Yamamoto, and T. Ando, "Tip-sample distance control using photothermal actuation of a small cantilever for high-speed atomic force microscopy," *Rev. Sci. Instrum.*, vol. 78, no. 8, pp. 083702-1–083702-5, Aug. 2007.

[28] L. E. Kinsler, A. R. Frey, A. B. Coppens, and J. V. Sanders, *Fundamentals of Acoustics*. New York: Wiley, 1982.

[29] B. Ohler, *Force Resolution in Force Spectroscopy Experiments: Thermal Noise and Bandwidth*. Plainview, NY: Veeco Instrum. Inc., 2007.

[30] L. Chen, C. L. Cheung, P. D. Ashby, and C. M. Lieber, "Single-walled carbon nanotube AFM probes: Optimal imaging resolution of nanoclusters and biomolecules in ambient and fluid environments," *Nano Lett.*, vol. 4, no. 9, pp. 1725–1731, Sep. 2004.

[31] P. C. Weber, D. H. Ohlendorf, J. J. Wendoloski, and F. R. Salemme, "Structural origins of high-affinity biotin binding to streptavidin," *Science*, vol. 243, no. 4887, pp. 85–88, Jan. 1989.

[32] J. Hyun, S. J. Ahn, W. K. Lee, A. Chilkoti, and S. Zauscher, "Molecular recognition-mediated fabrication of protein nanostructures by dip-pen lithography," *Nano Lett.*, vol. 2, no. 11, pp. 1203–1207, Nov. 2002.

[33] H. Torun, K. K. Sarangapani, F. L. Degertekin, and C. Zhu, "Parallel active polymer probes with integrated interferometer for single molecule force spectroscopy," presented at the Int. Meeting AFM Life Sci. Med., Monterey, CA, 2008.

[34] S. W. Stahl, E. M. Puchner, and H. E. Gaub, "Photothermal cantilever actuation for fast single-molecule force spectroscopy," *Rev. Sci. Instrum.*, vol. 80, no. 7, pp. 073702-1–073702-6, Jul. 2009.

**Hamdi Torun** received the B.S. degree in electrical and electronics engineering from Middle East Technical University, Ankara, Turkey, in 2003, the M.S. degree in electrical and computer engineering from Koc University, Istanbul, Turkey, in 2005, and the Ph.D. degree in electrical and computer engineering from the Georgia Institute of Technology, Atlanta, in 2009.

From 2002 to 2003, he was an Intern and then a Research and Development Engineer with Aselsan Inc., Ankara, Turkey. He is currently a Postdoctoral Fellow in the Department of Mechanical Engineering, Georgia Institute of Technology. His research interests include microsystems development for biological applications, atomic force microscopy, and thermomechanical infrared imagers.

**Krishna K. Sarangapani** was born in Chennai, India. He received the B.Tech. degree (with honors) in biotechnology and biochemical engineering from the Indian Institute of Technology, Kharagpur, India, in 2000, and the Ph.D. degree in bioengineering from the Georgia Institute of Technology (Georgia Tech), Atlanta, in 2005.

He completed his first postdoctoral stint in the Department of Mechanical Engineering, Georgia Tech, in April 2009. Since then, he has been a Senior Fellow in the Department of Physiology and Biophysics, University of Washington, Seattle. He has several publications in popular journals (*Journal of Biological Chemistry*, *Biophysical Journal*, and *European Biophysics Journal* to name a few), with more than 150 citations to date. His research interests include applying ultrasensitive force probe tools like the atomic force microscope and optical tweezers to study single biomolecular interactions.

Dr. Sarangapani is a recipient of multiple doctoral- and postdoctoral-level awards in recognition of his research efforts.

**F. Levent Degertekin** was born in Diyarbakir, Turkey. He received the B.S. degree from Middle East Technical University, Ankara, Turkey, in 1989, the M.S. degree from Bilkent University, Ankara, Turkey, in 1991, and the Ph.D. degree from Stanford University, Stanford, CA, in 1997, all in electrical engineering.

From 1992 to 1993, he was a Visiting Scholar in the E.L. Ginzton Laboratory, Stanford University, where he was an Engineering Research Associate from 1997 to 2000. Currently, he is a Professor in the George W. Woodruff School of Mechanical Engineering and the School of Electrical and Computer Engineering, Georgia Institute of Technology, Atlanta. He is also currently the George W. Woodruff Chair in Mechanical Systems at the Georgia Institute of Technology. He has authored 36 U.S. patents and over 150 scientific publications. His research interests include micromachined acoustic and optoacoustic devices, medical ultrasound imaging, bioanalytical instrumentation, and atomic force microscopy.

Dr. Degertekin was an Associate Editor for the IEEE SENSORS JOURNAL and currently is an Associate Editor for the IEEE TRANSACTIONS ON ULTRASONICS, FERROELECTRICS, AND FREQUENCY CONTROL. He is a member of the Technical Program Committee of the IEEE Ultrasonics Symposium. He was the recipient of a National Science Foundation Faculty Early Career Development (CAREER) award for his work on ultrasonic atomic force microscopy in 2004, and with his students, he was the recipient of the IEEE Ultrasonics, Ferroelectrics, and Frequency Control Society 2004 Outstanding Paper award.